FCT
Fundação para a Ciência e a Tecnologia
MINISTÉRIO DA CIÊNCIA, TECNOLOGIA E ENSINO SUPERIOR

Institute for Astronomy

School of Physics and Astronomy

University of Edinburgh

Estimating Star-formation at High-z

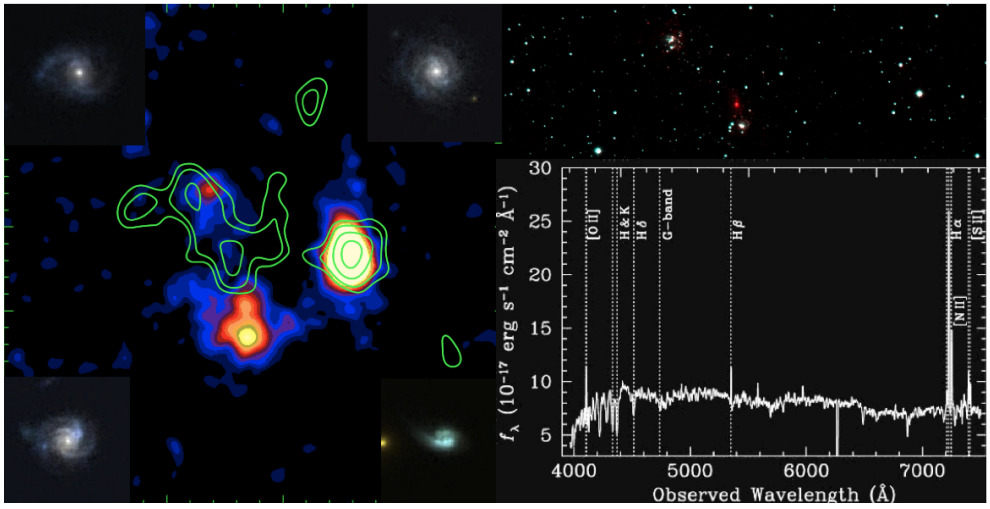

Pedagogical Seminar

David R. S. Sobral
drss@roe.ac.uk
www.roe.ac.uk/∼drss

30th March 2009

Contents

1 Introduction

In less than a few centuries, mankind was able to go far beyond the simple contemplation of the sky to a growing knowledge of the Universe. It has not been an easy task, and few can say that the journey has been undertaken without any major surprises. From dark matter and its huge importance in the formation and evolution of galaxies, to the mysterious dark energy, apparently driving the accelerated expansion of the universe, every discovery, near and far, brought more and more challenges. On the other hand, the immense technological development, driven by intensive research and an increasing understanding of the physics of our World, is definitely pushing us forward. Large and sophisticated telescopes are now fully working, while better and bigger ones are constantly being planned and built. Thus, with multi-wavelength data analyzed and produced across the globe (together with powerful models and simulations), we still don't have the key to unveil the complete history of our Universe, but we believe we have found the tools and the path that can lead us there.

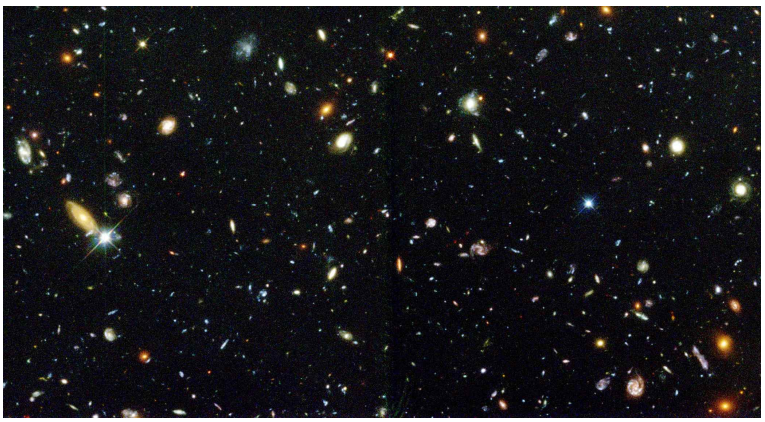

Fig. 1: Hubble Deep Field: the deepest optical image ever made gives us the best view of the Universe thousands of millions of years ago.

1.1 Galaxy Formation

It is believed that galaxies form as a result of gravitational collapse due to instabilities caused by density perturbations in the early Universe. These density perturbations are observed as fluctuations in the Cosmic Microwave Background. On the other hand, Inflation, the concept that the universe underwent a rapid period of expansion at an early age, is probably the best natural candidate for these seed fluctuations. The inflationary expansion would have both amplified and frozen quantum fluctuations in the density field. The collapse of these density perturbations can then continue in either one of two ways: top down or bottom up (hierarchical) formation. The way in which galaxies form depends greatly on the cosmological parameters and the nature of the matter involved.

Matter is often divided into two groups: baryonic matter and dark matter. The latter has a non-luminous nature, thus we can only infer its existence by gravitational effects on stars in galaxies, or on galaxies in clusters. So far, several dark-matter candidates have been proposed, yet none has been confirmed. Nevertheless, cold dark matter (CDM) seems to be one of the best candidates. CDM consists of massive particles which are non-relativistic at the point at which they decouple from the rest of matter and radiation (in the early Universe).

Nowadays, N-body simulations can be used to model the history of dark matter in the universe by finding numerical solutions to the coupled equations of the gravitational interactions of N particles (of dark matter). These simulations are the roots for current cosmological simulations. Coupled with these N-body simulations one can perform full hydrodynamic calculations with semi-analytical models which allow the modelling of how the gas interacts with the dark matter to form galaxies. Star-formation, feedback and metal enrichment can also be included in order to achieve more accurate results.

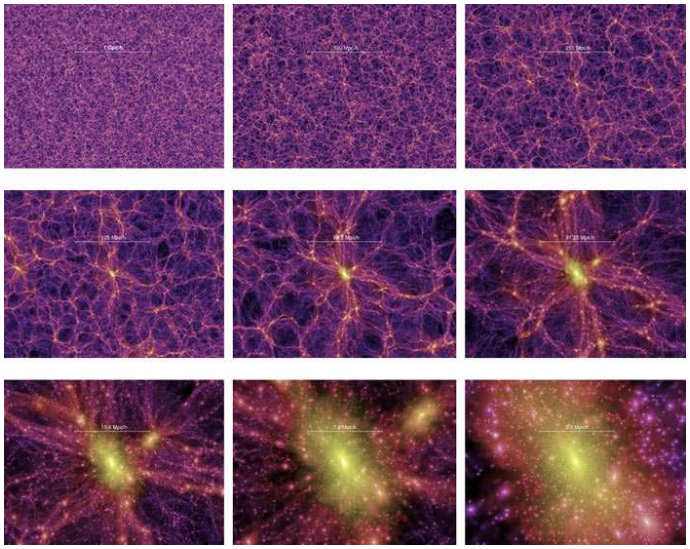

Fig. 2: A view of the millennium simulations at different scales, revealing the structure predicted nowadays, which matches well most of the observations done so far.

Running CDM simulations reveals a Universe which develops in a bottom-up scenario. This means stars form early and galaxies form first, before developing into clusters and super-clusters by a series of complicated merging episodes. These predictions fit the observed universe quite well. Also, given the consensus on cosmological parameters, the appropriate models are refered to as Λ-CDM models, which is, at the moment, the most popular model. However, there are still some flaws within this models. Whilst they fit the general observations well, implying that the ingredients of the model are essentially correct, there are some classes of objects which cannot be properly explained. For example, they under-predict the number of Lyman-break galaxies and sub-mm galaxies at high-redshift. These problems are not necessarily fundamental: there are sufficient dark matter haloes produced to house these massive galaxies at high redshift. In fact, global properties such as the global star-formation rate and the total co-moving stellar mass are reasonably well matched as a function of redshift. However, it is clear that the physical mechanisms for star-formation are not yet fully understood. One particular example is the fact that there is enough stellar matter predicted at high redshift, but not in the form of large, red spheroids. Feedback mechanisms that allow the quenching of star-formation have now been introduced in an attempt to solve these problems and AGN may well drive this feedback.

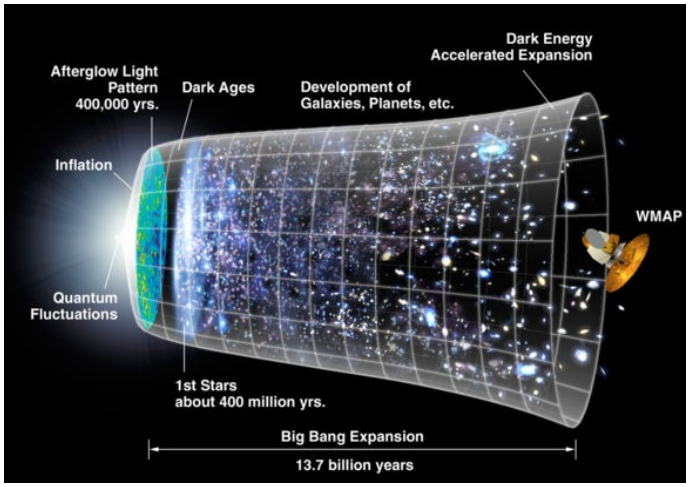

Fig. 3: A summary-view of the main evolutionary steps in the history of the Universe – from the Big Bang to the present day.

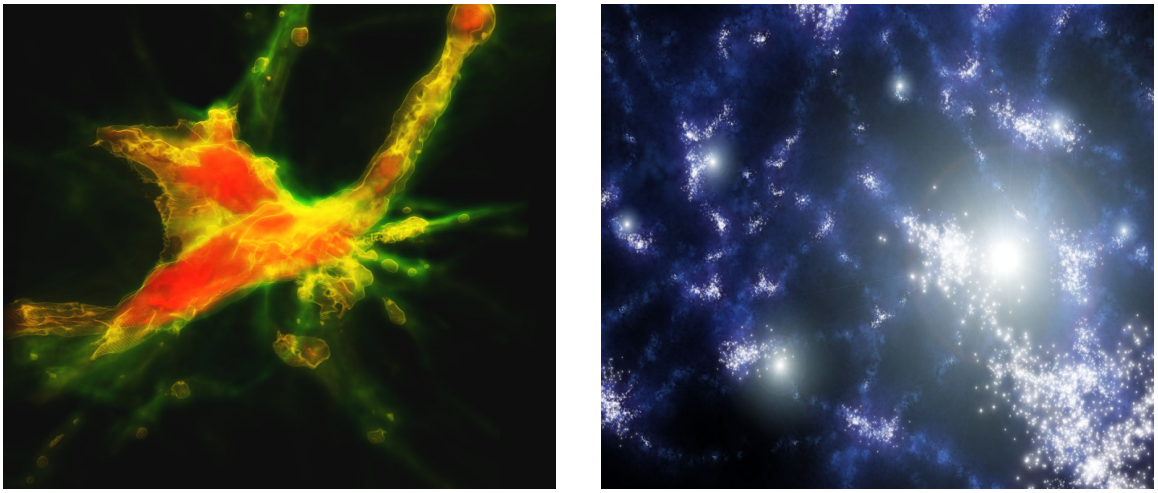

Fig. 4: The $left$ panel shows a simulated galaxy at $z = 10$, sites of the first star-formation episodes in the Universe; the $right$ panel presents an artist impression of the first stars – the $metal\text{-}free$ population III. These stars are expected to have been very massive (∼100 times as massive as the sun) and extremely short-lived, contributing significantly to the re-ionization of the Universe.

1.2 The First Light: Population III

The formation of the first stars at redshifts z ∼ 15-20 is thought to have marked an extremely important transition in the history of the Univese. With the formation of the first luminous objects, the universe was rapidly transformed into an increasingly complex, hierarchical system, due to the energy and heavy element input from the first stars and accreting black holes. Those stars are thought to have formed just 150 Myr after the Big Bang, when the primordial gas was first able to cool and collapse into dark matter mini-halos with masses of $\sim 10^6$ $M_\odot$. Those stars formed in a very different environment when compared with the present star-formation. In fact, due to the lack of metals, the cooling mechanisms are so ineffective (the main cooling mechanism is through H_2 molecules) that they seem to imply the production of stars with $\sim$ 100 $M_\odot$. Nevertheless, it is still not clear whether those very massive objects would be able to fragment into smaller ones, although recent studies have shown that it is not likely to happen. Whilst being so massive, they are expected to have been extremely luminous, thus being able to effectively contribute to the reionization of the Inter-Galactic Medium (IGM). The first clouds to collapse could also result in the direct formation of the first black holes with masses of $\sim$ 10 $M_\odot$ which could then grow quite rapidly. This can then explain how it is possible to find "super"-massive black holes at very high redshift (z ∼ 6-7).

2 Star-forming Galaxies and Star Formation

Understanding the basic features of galaxy formation and evolution requires unveiling a quantity which we shall call volume-averaged star formation rate density, ρ_{SFR}; this provides a measurement of how many stars per unit volume the Universe was forming at a particular epoch – understanding its evolution with cosmic time unveils the star-formation history of the Universe and how it assembled its stellar mass.

In the local Universe, studies have demonstrated that star formation is strongly dependent on the environment. While clusters of galaxies seem to be primarily populated by passively-evolving galaxies, star-forming galaxies are mainly found in less dense environments. Star-forming galaxies have also been found to have lower masses than passive galaxies. How do these environmental and mass dependencies change with cosmic time? When did they start to be noticeable, and how do they affect the evolution of galaxies, clusters and the star formation rate density of the Universe as a whole? How much of the evolution of the cosmic star formation rate density is associated with the evolution of star-forming galaxies and how much is driven by galaxy merger activity?

In order to properly answer such questions it is mandatory to conduct observational surveys at high redshift,

which can then be used to test theoretical models of galaxy evolution. However, such surveys can only be carried out provided that we have the right tools for both selecting significant samples of star-forming galaxies, and measuring how much star-formation is on-going in each of those.

2.1 Measuring Star-formation

Most of the baryonic mass in a galaxy is in the interstellar medium. Eventually, this can build clouds of gas, where structure can form due to turbulence and/or activity of other stars. Random turbulent processes can then lead to regions which are dense enough to collapse under their own weight, these can then form stars. However, as soon as we leave our own galaxy, the distances involved become so large that it becomes extremely difficult to probe star formation in an individual-cloud basis. The best we can do – even with the high-resolution of the Hubble Space Telescope – is obtain an average star-formation rate across the entire galaxy using different star-formation rate tracers which reveal the $signatures$ of recent star-formation.

Fig. 5: HII regions are associated with intense star-formation. This image shows a HII region within our galaxy with the Hα emission shown in red – this is a result of the strong ionizing radiation from massive stars.

2.2 Initial Mass Function

Probing star formation in distant galaxies and trying to obtain a reliable star-formation rate is not an easy task. As the following sections describe, the really $distinct$ signature of recent star-formation activity comes from newly born massive stars (which are short-lived). Can we extrapolate the signature of those massive stars to lower mass stars and determine the total star formation rate? Yes, if we know the initial mass function.

The initial mass function, IMF, is an empirical function that tries to describe the mass distribution of stars as a function of their theoretical initial mass that led to their formation. It is often represented by $\xi(M)$ and is frequently written as simple power law:

$$\xi(M) = cM^{-(1+x)} \tag{1}$$

In general, however, $\xi(M)$ is assumed to extend from a lower to an upper cutoff, normally chosen to be $M_1 = 0.1\mathrm{M}_\odot$ and $M_2 = 100\mathrm{M}_\odot$.

The three most used IMFs are the Salpeter (1955), the Miller & Scalo (1979) and the Scalo (1986) laws. Those three IMFs are plotted in figure 6. The different slopes of the considered laws produce different spectral energy distributions. The Scalo (1986) and Miller & Scalo (1979) are flat at small masses and less rich of massive stars

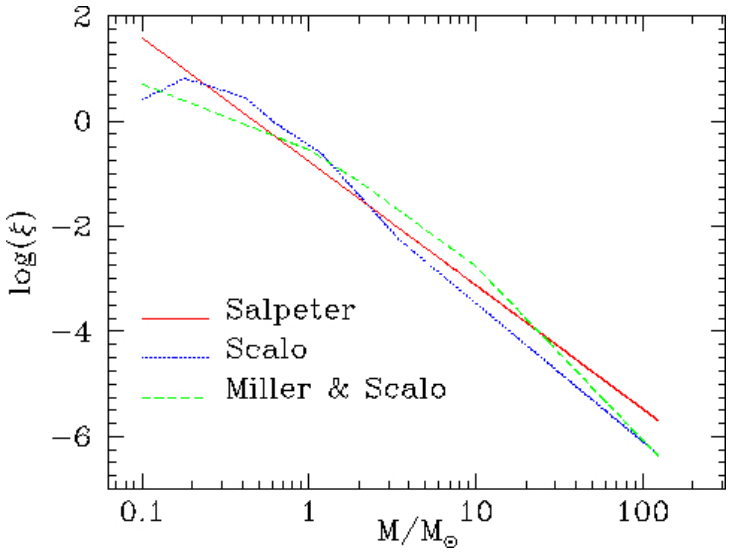

Fig. 6: The three most used IMFs: Salpeter (1955), Miller & Scalo (1979) and Scalo (1986).

Tab. 1: Main Sequence lifetimes and typical masses.

Star	$M_\odot$	Lifetime
O3	60	3 Myr
O7	30	11 Myr
B4	10	30 Myr
A5	3	0.3 Gyr
F5	1.5	3 Gyr
G2	1	10 Gyr
M7	0.1	1 Tyr

with respect to the Salpeter (1955) IMF, as they allow x to vary in different mass ranges. Salpeter (1955), on the other hand, implies a large number of massive stars, producing an excess of UV flux, whereas the Scalo (1986) law generates too many solar mass stars, making the spectrum too red to match observed colours.

Several studies have been done in our galaxy, where we can probe star-forming regions in detail. These have shown that the IMF remains fairly constant for all the regions studied, i.e., for each star-forming region, the fraction of stars forming with a given mass as a function of the initial mass of the cloud does not change considerably. Therefore, for years now, astronomers have assumed a constant IMF which has been empirically determined.

Nevertheless, while the constancy of the IMF within our galaxy seems to valid, the same might not be true for star-forming regions in other galaxies, particularly when one looks at star formation in very massive or/and very young galaxies at high-redshift.

2.3 Estimating Star-formation: SF indicators

The "current" star formation rate (SFR) of a galaxy is a fundamental parameter for our understanding of galaxy evolution. There are several ways we can estimate star formation rates, with these $tracers$ being at different wavelenghts. From the continuum ultraviolet (UV) radiation, directly generated by those stars, to major emission lines in the visible (such as Hα and [OII]) and to far-infrared or radio luminosities, massive, newly-born stars or their deaths generate specific signatures that we can detect and interpret.

Ideally, the use of different star formation tracers would provide consistent answers to most of the questions that remain unanswered. Unfortunately, with different star formation tracers suffering different biases and selection effects, significant discrepancies are found. These problems are also amplified by the effects of cosmic variance

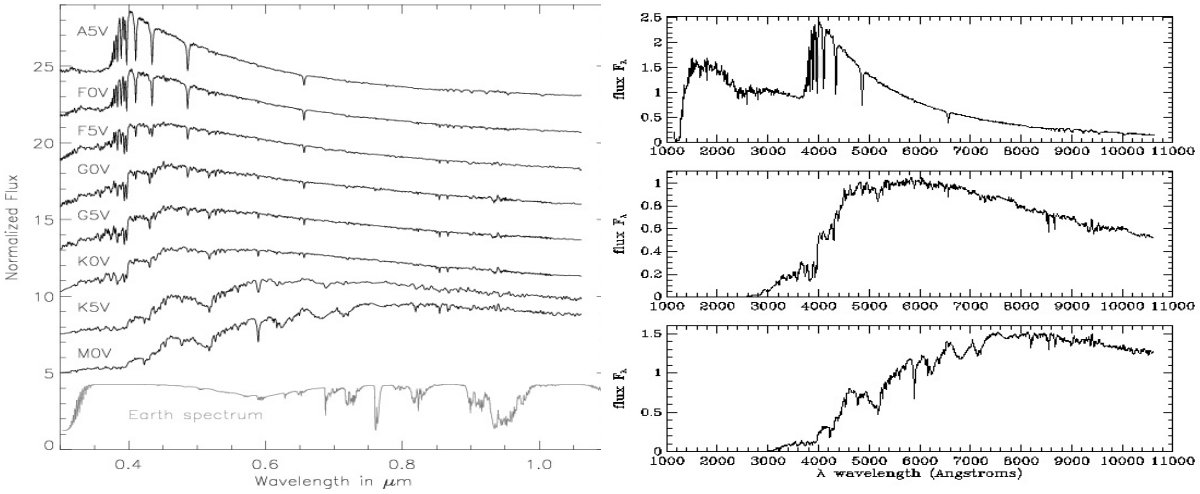

Fig. 7: Spectra for typical stars with decreasing mass from the top to the bottom and a comparison with Earth's spectrum($left$), showing that only the most massive stars contribute significantly to the UV flux. The $right$ panel presents details of these stars, emphasizing that at ∼100-250 nm the emission the UV emission is completely dominated by massive stars which are very short-lived.

in most of the current samples. Another issue is the difficulty in correcting for extinction, especially for UV and optical wavelengths, which can lead to large systematic uncertainties in the star formation densities derived from measurements in these wavebands.

No single indicator provides a perfect view of the evolution of the star-formation rate density; each has its biased view, together with advantages and disadvantages.

2.3.1 Ultraviolet Continuum

Massive, newly born stars are characterized by a very intense UV light (see Figure 7). On the other hand, as these stars are very short-lived (see Table 2, showing that the lifetime scales as $\sim M^{-3}$), the amount of UV light can then be used as an "instantaneous" star formation rate (SFR) tracer. In order to avoid contamination by older stars, the optimal wavelength range is 125-250 nm, longward of the Lyα forest. These wavelengths are inaccessible from the ground for local galaxies (z<0.5) but one can easily observe these in the redshift range 1-5. The conversion between UV flux over a given wavelength interval and the SFR can then be derived using synthesis models. Assuming a constant SFR over time scales long enough when compared to the lifetimes of dominant UV emitting population (∼10-50 Myr), and using a Salpeter (1955) IMF with mass limits 0.1 and 100 $M_\odot$ yields:

$$\mathrm{SFR}(M_\odot \mathrm{year}^{-1}) = 1.4 \times 10^{-28}\ L_\nu\ (\mathrm{ergs.s}^{-1}\mathrm{Hz}^{-1}) \quad (2)$$

Unfortunately, UV is very sensitive to extinction and to the form of the IMF. Typical extinction corrections in the integrated UV magnitudes are 1-3 mag, but these can be even higher for very dusty galaxies.

While UV luminosity is commonly used as a SFR indicator, the luminosity at u-band wavelenghts (λ ∼3600Å) is similarly dominated (in starburst galaxies) by young stellar populations, and in the absence of UV measurements it may be used as a SFR indicator. The dust-extinction corrections range from 3 to 10 for typical star-forming galaxies. However, using u-band as a SFR indicator is more problematic than UV; it is harder to assign a simple scaling factor to derive a SFR due to the strong dependence on the evolutionary timescale. From synthetic galaxy spectra it can be seen that the u-band luminosity varies from about a factor of 10 lower than the UV luminosity at the onset of a burst of star formation to almost equivalent on later times.

Given this sensitivity of the u-band luminosity (L_u) to the starburst age and the assumed star formation history, a more complex calibration is in general likely to be necessary. This may take the form of a nonlinear dependency

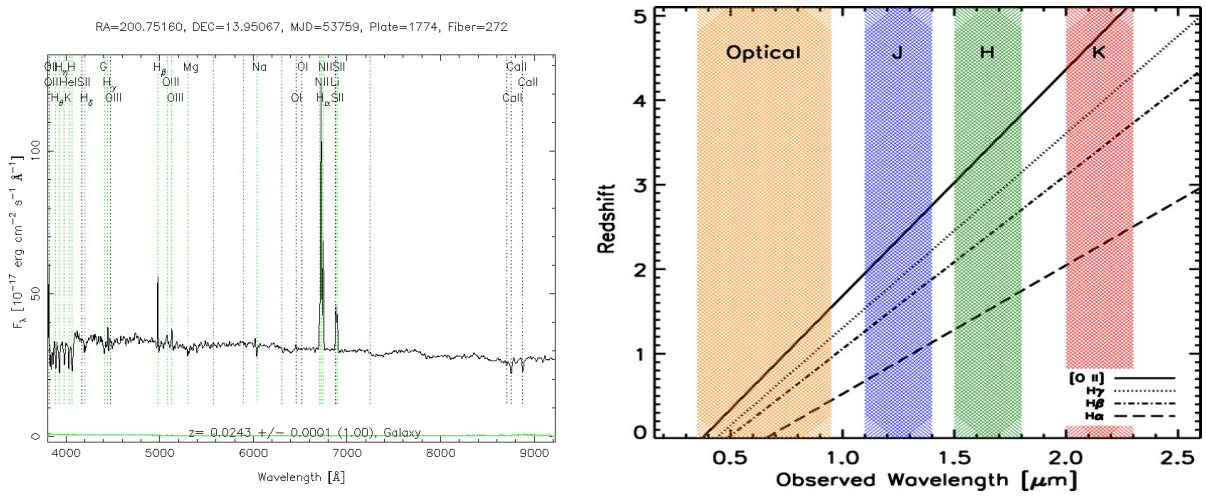

Fig. 8: $Left$: A typical spectrum of a low-redshift starburst galaxy, showing strong Hα, Hβ and [OII] emission lines. At higher redshifts, these lines move to higher wavelengths and can only be observed in specific windows ($right$), with the Hα line being the first to go beyond the K band, at z$\sim$2.5.

on L_u to reflect the rapid change of L_u with respect to L_{UV} during the first 10^8 yr of a starburst and to account for the presence of old stellar populations that are likely to contribute significantly to L_u in less luminous systems. More quiescent or low-luminosity SF systems have a relatively larger contribution to their u-band luminosity from old stellar populations (they are, on average, redder than more luminous galaxies), and this causes a linear calibration from luminosity to SFR to result in an overestimation.

While recent star-formation activity is likely to produce large quantities of energy, initially released by the massive young stars, a significant portion of that energy is actually absorbed and re-emitted through a large variety of physical processes, including emission lines. Therefore, while the UV luminosity is the only $truly\ direct$ star-formation indicator, the advantages of the following SF tracers can, in many cases, make them a better choice than UV.

2.3.2 Emission lines: Hα, [OII] and others

Only stars with masses of $> 10\ M_\odot$ and lifetimes of < 20 Myrs (OB stars) contribute significantly to the integrated ionizing flux, so emission lines provide a nearly instantaneous measure of the SFR, independent of the previous star formation history. With most of the baryonic matter being in the form of Hydrogen, this is the element that tends to absorb most of the UV photons. The following de-excitation of hydrogen atoms then happens through a broad range of processes. One of the most common ways implies the emission of photons of the Paschen series. Hα photons are also emitted quite effectively. The latest are much less sensitive to dust extinction than UV, and the Hα emission line is strong enough to be detected at very large distances both spectroscopically or using narrow-band surveys in the visible or infra-red bands. Despite that, it is still affected by extinction, which one can account for by measuring the flux of Hβ, for example. This works due to the existence of a standard Hα to Hβ ratio for photo-ionisation, thus measuring the observed ratio probes the effective extinction. Nevertheless, this is a hard task, as Hβ is often weak and hard to detect or measure. For solar abundances, and the same Salpeter IMF (0.1 to 100 $M_\odot$), the calibrations of Kennicutt et al. (1994) and Madau et al. (1998) yield:

$$\mathrm{SFR}(M_\odot \mathrm{year}^{-1}) = 7.9 \times 10^{-42}\ L_{H\alpha}\ (\mathrm{ergs.s}^{-1}) \tag{3}$$

Large Hα surveys have been published since de 70's, using narrow-band imaging and spectroscopy. Hα also permits the mapping of nearby galaxies at high resolution, even with smaller telescopes. Nevertheless, it is still

sensitive to uncertainties in the IMF, along with the assumption that all of massive star formation is traced by ionized gas. Integrated Hα and radio fluxes of galaxies have been used to derive a mean extinction A(Hα) = 0.8-1.1 mag. As mentioned before, Paschen and Brackett lines are also involved in the recombination process, and thus can potentially be used as SFR tracers. However, they are typically 1-2 orders of magnitude weaker than Hα and can only be used for the brightest emitters.

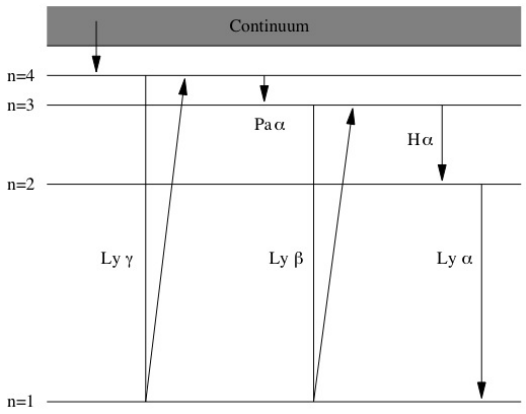

Fig. 9: A schematic view on some of the recombination emission lines for hydrogen, with Hα ending up being one of the strongest (from $Philip\ Best's$ lecture notes).

The Hα line is redshifted out of the visible window for z >0.5, so bluer lines which can trace SFR can be very important. Unfortunately, the other Balmer lines are poor SFR diagnostics, as they are both weak and very stellar-absorption dependent, but other elements, such as oxygen, can play an important role. In fact, one of the strongest emission features in the blue is the [OII]$_{\lambda\lambda 3727}$ doublet emission line (forbidden). Luminosities of forbidden lines are not directly coupled to the ionizing luminosity, and their excitation is sensitive to abundance and the ionization of the gas. Despite that, the excitation of [OII] is sufficiently well behaved and it can be empirically calibrated using Hα as a quantitative SFR tracer. As [OII] falls into the visible window out to redshifts of about 1.6, it can easily be used for large surveys up to that redshift . Only the hottest stars have sufficient UV flux to ionize oxygen atoms, therefore the [OII] flux is mostly due to O and B stars. Rates of star-formation come from folding in the well-known lifetimes of those stars. Adopting the same IMF and calibrating using Hα emission results in:

$$\mathrm{SFR}(\mathrm{M}_{\odot}\mathrm{year}^{-1}) = (1.4 \pm 0.4) \times 10^{-41}\ \mathrm{L}_{[\mathrm{OII}]}\ (\mathrm{ergs.s}^{-1}) \tag{4}$$

where the uncertainty indicates the range between blue emission-line galaxies (lower limit) and samples of more luminous spiral and irregular galaxies (upper limit). Observed luminosities must still be corrected for extinction, in this case the same as Hα due to the calibration used. Unfortunately, SFRs derived by this method are less precise than those using Hα, especially because the line ratio between both lines varies considerably from galaxy to galaxy. However, it is very useful, especially for consistency check on SFRs derived with other methods.

2.3.3 Far-Infrared Continuum

A large fraction of the bolometric luminosity of a galaxy is absorbed by interstellar dust and re-emitted in the thermal IR at wavelengths of roughly 10-300μm. The involved cross-section is strongly peaked in the UV, implying that the far infrared (FIR) emission can be a sensitive tracer of the young stellar population and SFR. In fact, the efficiency of this method depends on the contribution of young stars to heating the dust and on the optical depth of the dust in star-forming regions. The simplest physical situation occurs when young stars dominate the radiation field in the UV-visible and the dust opacity is high everywhere. In this case, the FIR luminosity measures the

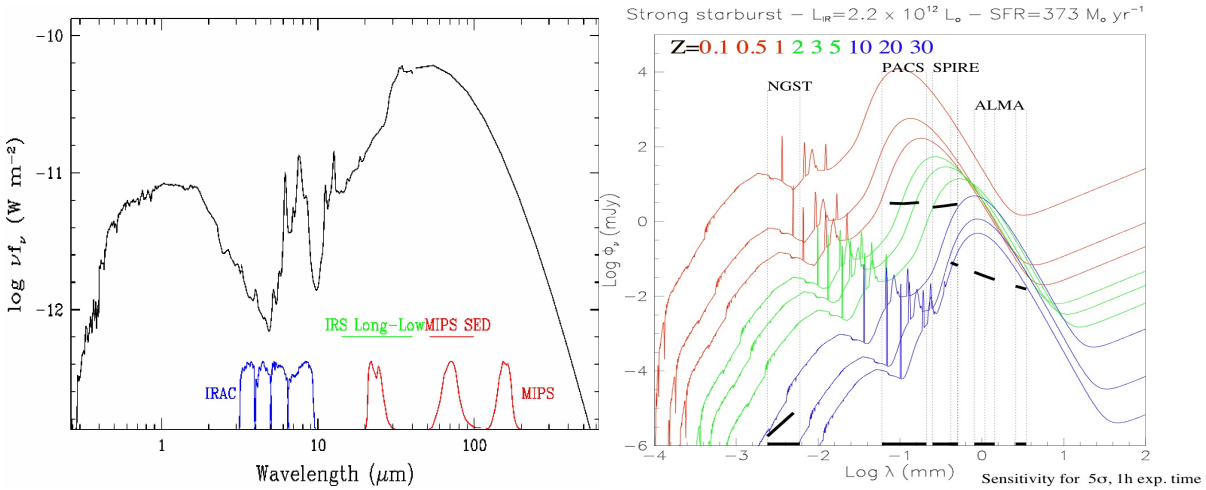

Fig. 10: The spectral energy distribution of a typical star-forming galaxy ($left$) and the evolution with redshift ($right$). The interstellar dust absorbs the UV light from young stars and radiates like a blackbody in the mid-infrared, with that radiation being typically strong enough to be detected and measured.

bolometric luminosity of the star-formation $burst$. In such a limiting case, the FIR luminosity is an excellent SFR tracer, providing a calorimetric measure of the SFR. Such conditions roughly hold, at least in the dense circum-nuclear starbursts that power many IR-luminous galaxies, though the physics become more complex when dealing with disks of normal galaxies. In fact, the FIR spectra of galaxies contain both a $warm$ component associated with dust around star-forming regions ($\sim \lambda = 60$ μm) and a $cooler$, $infrared\ cirrus$ component at longer wavelengths which is associated with more extended dust heated by the interstellar radiation field. In blue galaxies, both spectral components may be dominated by young stars. However, for red galaxies, where the composite stellar continuum drops off steeply in the blue, dust heating from the visible spectra of older stars may be important.

The relation between the global FIR emission and the consequent SFR has been a controversial subject. On one hand, it is true that for late-type galaxies, where dust heating from young stars is expected to dominate the 40 to 120 μm emission, the FIR luminosity correlates well with other SFR tracers such as the UV continuum and Hα luminosities (Buat & Xu, 1996). On the other hand though, early-type galaxies often exhibit high FIR luminosities, but much cooler, cirrus-dominated emission.

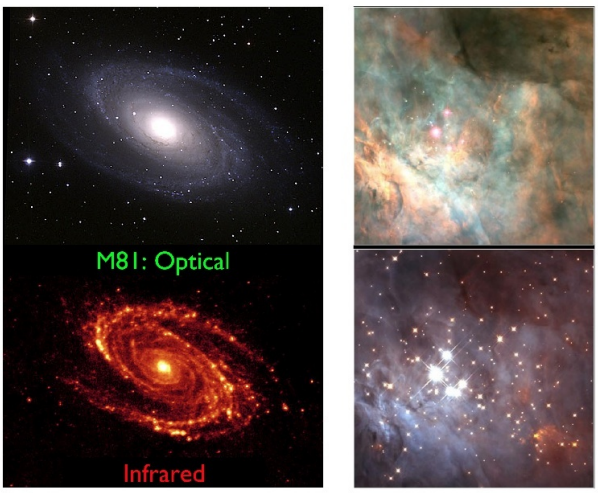

Fig. 11: The optical $versus$ infrared view of M81 and a star-formating region showing how dust extinction can alter the view of the same exact objects.

Despite the problems one finds when calibrating the FIR as a SFR tracer, the truth is that it should provide an excellent measure of the SFR in dusty circum-nuclear star-bursts. Calibrations published by Kennicutt (1998) using the same IMF as before yields the relation:

$$\mathrm{SFR}(\mathrm{M}_{\odot}\mathrm{year}^{-1}) = 4.5 \times 10^{-44}\, \mathrm{L}_{\mathrm{FIR}}\ (\mathrm{ergs.s}^{-1}) \tag{5}$$

where $\mathrm{L}_{\mathrm{FIR}}$ is obtained by integrating over the full, mid and far-IR spectrum (8 to 1000 μm). Nevertheless, for starbursts, most of the emission will happen in the 10 to 120 μm range. In practice, obtaining the far-IR integrated spectrum implies SED fitting using the most commonly-used bands, where the 24 μm (MIPS) and the sub-mm bands are powerful (and essential) tools.

2.3.4 Radio

Long-wavelength SFR estimates are insensitive to dust obscuration, increasing their attraction for SFR investigations, but they are not without limitations. Radio luminosity can be generated by AGN as well as star formation processes, and indeed the majority of apparently bright radio sources are AGNs. By selecting for star formation directly from optical spectroscopic features, however, one can eliminate this potential source of confusion. The detailed physics involved in the connection between SF and radio emission is still poorly understood, despite numerous attempts. Still, and neglecting AGN radio-sources, there are two main components of the radio continuum emission in star-forming galaxies: thermal $bremsstrahlung$ from ionized hydrogen in HII regions and nonthermal synchrotron emission from cosmic-ray electrons (from supernovae events) spiraling in the magnetic field of the galaxy. Thermal radio emission presents a spectrum $\sim \nu^{-0.1}$, whereas non-thermal emission presents a steeper spectrum with $\sim \nu^{-0.8}$.

Because radio is essentially not affected by extinction, it is often regarded as a good SFR tracer (although not an $instantaneous$ tracer, as it mostly probes supernovae events, and thus it can be considered a $delayed$ SFR indicator), especially for the most obscured, dusty galaxies (but not very sensitive).

Radio emission is also well correlated with the FIR emission, even though the broad range of different physical processes involved would not imply it. In fact, it has proven to be one of the tighter relations in astronomy, and recently, Ibar et al. (2008) have shown that it still holds even for high redshift.

2.3.5 Gamma-ray bursts

We have seen before that it is possible to infer the formation rate of massive stars from their death rate, since their lives are short. While it is not possible to detect ordinary core-collapse supernovae at high redshift, long-duration gamma-ray bursts, which have been shown to be associated with a special class of core-collapse supernovae, have been detected almost as far as $z \sim 7$. Therefore, assuming that it is possible to match the number of these GRBs with an average star-formation rate density at a particular epoch, one can try to obtain a star-formation history of the Universe based on them. Nevertheless, while the calibration is not easy to obtain, GRBs are also too rare to provide the same amount of information as all the other SFR indicators described before.

2.3.6 X-Rays

Binary systems with two very massive stars can evolve to form high-mass X-ray binaries, these are generally more powerful than Supernovas and their remnants. There are actually two types of X-ray binaries: low mass X-Ray binaries (LMXBs), which contain a neutron star or a black hole as the primary object, together with a star of less than 2.5 $\mathrm{M}_{\odot}$, and high-mass X-ray binaries (HMXBs) with a secondary object of more than 2.5 $\mathrm{M}_{\odot}$. This results in very different lifetimes, together with a significant difference in the accretion – stars in HMXBs have strong stellar winds and thus the primary can accrete mass from this wind alone. Also, as HMBXs present lifetimes of

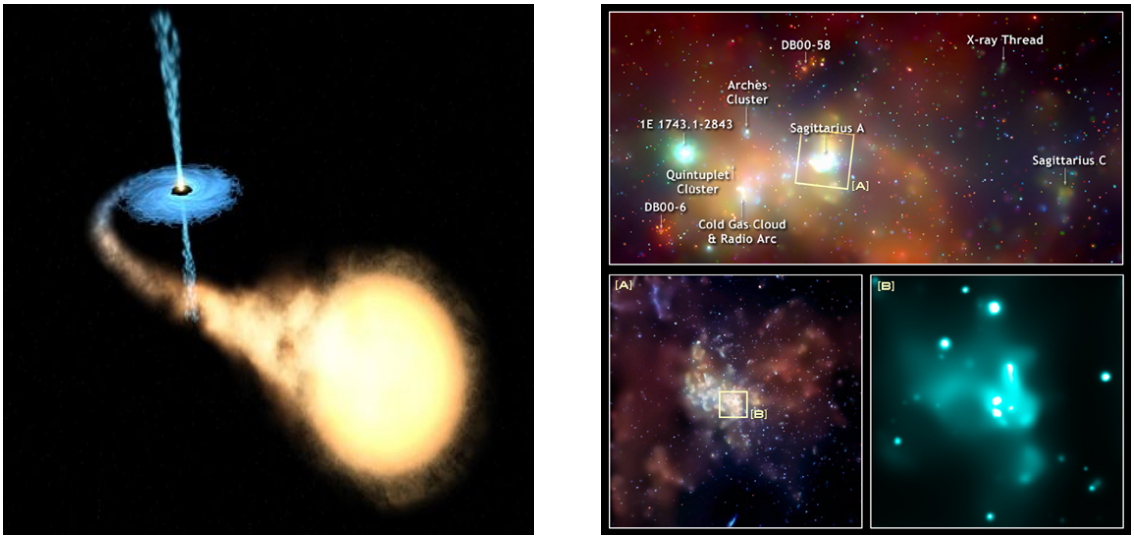

Fig. 12: An artist impression of a HMXB, with the black hole being the primary object, accreting from the star. The gas then heats up when spiraling towards the black hole, which then results in X-ray emission detectable from space ($left$). The $right$ panel shows X-ray imaging of our galaxy, with most of the point sources in the image being LMBXs.

10^5-10^7 years, they can, in principle, be used as a good recent star formation indicator. The X-ray emission from HMXBs can penetrate thick columns of gas and dust to give an unobscured view of the star-formation activity.

However, for distant galaxies, it is not really possible to distinguish between the X-ray contribution of LMXBs and HMXBs. Still, using some other star-formation indicator to select apparent star-formation dominated galaxies, one can in principle assume that most of the X-ray flux is actually coming from HMXBs and not from LMXBs (which are related to the mass of the galaxy) and in some cases obtain an X-ray based star-formation rate.

2.4 Observing: a practical view

Having mentioned the main star-formation indicators and some details about them, we should now look at how to use those in practice. We have already mentioned before that some tracers can only be used in a certain redshift window, mostly because of the atmospheric limitations. While the main physical quantity that one needs to get a star formation rate is $luminosity$, the actual quantity that one usually obtains is flux (see Appendix). The main "techniques" used are:

- $Broad\text{-}band\ imaging$:

  Broad-band imaging can be an effective way to detect faint galaxies - specially if the imaging is done from space in a telescope such as Hubble, or from the ground with 8-m class telescopes. More than being an important piece of information in itself (e.g. probing the redshifted UV continuum), broad-band imaging is also widely used to estimate the redshift of distant galaxies (using data from various different filters), which is extremely important to obtain a luminosity; without a distance estimate any star-formation indicator is meaningless.

  $Telescopes$: Almost all telescopes (e.g. Keck, Subaru, Hubble) with imaging capabilities and broad-band filters can be used for this. However, the main target is usually the redshifted UV continuum, which, depending on the redshift, can be obtained using several different bands. For mid-infrared imaging, on the other hand, one needs to go to space, with Spitzer being the best contributor to this in the last few years.

- $Narrow\text{-}band\ imaging$:

Narrow-band emission-line surveys are very effective for obtaining Hα and/or [OII]-derived star-formation rates for large and robust samples of galaxies. Moreover, with the "rise" of large-format imaging cameras in the optical and in the near-infrared, narrow-band filters can be used to undertake deep and unbiased surveys for emission-line objects in large volumes at the most important redshifts (out to z$\sim$2.5 for Hα). The surveys identify the sources on the basis of the strength of their emission line and thus represent a star-formation rate-selected sample, while they also select very narrow redshift slices. Hence, by using a set of narrow-band filters, it is possible to apply a single technique to target Hα emitters across a wide range of redshifts, gathering representative samples at each epoch with a uniform selection.

$Telescopes$: Almost all telescopes with imaging capabilities and narrow-band filters can be used for this (e.g. VLT, SUBARU, UKIRT). Different narrow-band filters target different emission lines – but a single filter can target more than one emission line (Hα and [OII] at different redshifts, for example).

- *Spectroscopy*:

  Spectroscopy is a powerful tool: not only does it allow us to determine the galaxy's redshift (so the distance can be accurately determined, which is not necessarily the case when one uses broad-band photometry alone), but it can provide the opportunity to measure line fluxes of more than one line (Hα and [OII] at the same time, for example). However, it can be very time consuming and not always the best approach to obtain SFRs at particular redshifts.

  $Telescopes$: A significant portion of telescopes have spectrographs that can be used to obtain spectra (e.g. VLT, Keck, GEMINI). While traditionally these would only target one galaxy at a time, at the present one can easily target dozens to hundreds of galaxies at the same time, wither using fibers of slits.

- *Sub-mm/Radio imaging*:

  Radio telescopes work in a significantly different way from optical/infrared telescopes due to the different wavelengths that they probe. These include the largest telescopes in the world, with single collector plates of $\sim$100 m. On the other hand, interferometry has been widely used at these wavelengths for years now, making combinations of many radio telescopes into an effective large telescope capable of reaching fainter and obtaining a detailed view of the sources being targeted.

  $Telescopes$: The best radio telescopes include the VLA, GRMT or the VLBA, with the JCMT being the largest in the sub-mm.

2.5 Star-forming Galaxies vs. AGN: how to distinguish them

Starburst galaxies are characterized by intense star formation periods (with star formation rates from $\sim 10\ M_{\odot} yr^{-1}$ to $\sim 1000\ M_{\odot} yr^{-1}$. They are rich in high mass stars - higher than 8 $M_{\odot}$, with short mean lifetimes $\sim 10^7$ years, which contribute to a high rate of supernovae events. The cosmic rays produced will then interact with the galaxy magnetic field, producing synchrotron radiation, a process that lasts for at least $\sim 10^5$ years. Typical star-forming galaxies present star formation rates slightly lower than that, but their spectra are very similar to those of starburst galaxies, with the same main emission lines (although these are not as strong).

Active galactic nucleus (AGN) are galaxies which host a super-massive black hole in their nucleus. The later is responsible for accelerating electrons and thus it is a very important source of radio radiation, although not all AGN are radio sources. On the other hand, we can distinguish between various types of AGN. Quasars (Quasi Stellar Objects) present strong emission lines, most of them broad (as they are produced near the nucleus, where density if higher, and the gas is moving faster), and they are distributed at high redshifts, even though they look as bright as some of the closest objects we can observe. Seyfert galaxies also present strong emission lines. However,

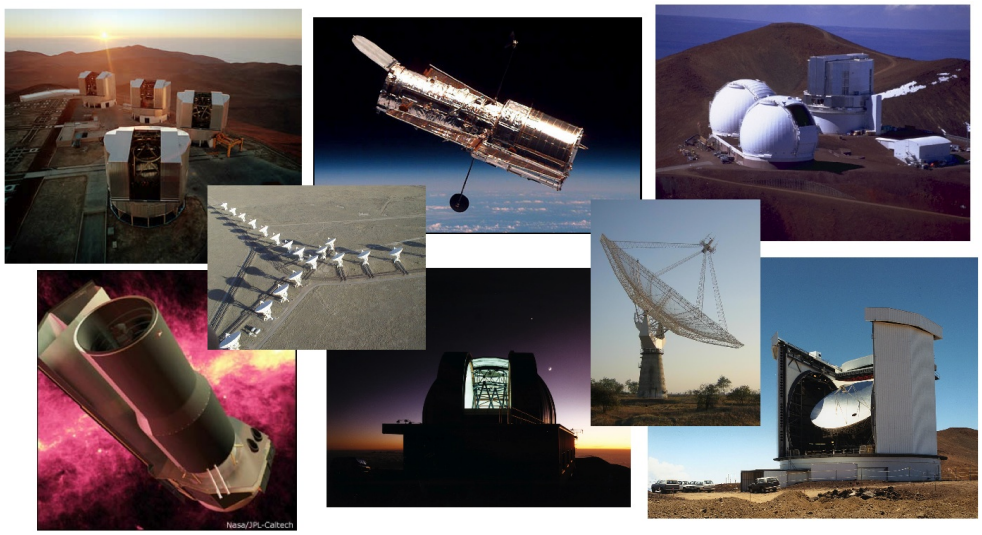

Fig. 13: Some of the largest and more significant telescopes ever built. Top (left to right): Very Large Telescope (VLT, visible and near-infrared), Hubble Space Telescope (HST, near-UV, visible and near-infrared), Keck and Subaru telescopes (visible and near-infrared). $Middle$: Very Large Array (VLA, radio), Giant Metrewave Radio Telescope (GMRT, radio). $Down$: Spitzer (mid-infrared), United Kingdom Infrared Telescope (UKIRT), James Clerk Maxwell Telescope (JCMT, sub-mm).

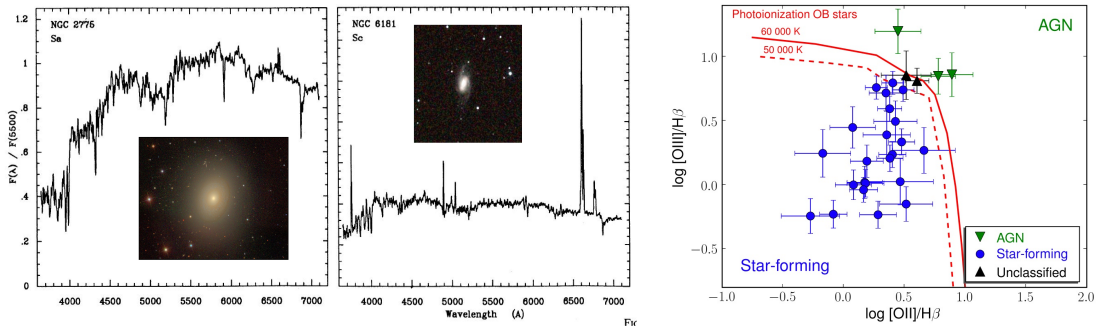

Fig. 14: AGN can easily be distinguished from star-forming galaxies when they present mostly absorption features typical of an old and red population of stars ($left$ panel). However, AGN can also present visible spectra which resembles those of star-forming galaxies – for those cases, line ratios can be used, as the ionizing sources are significantly different.

while being fainter, they can also be divided into two separate classes: Seyfert I and II. The first group includes galaxies presenting broad emission lines (the permitted emission lines, together with the forbidden emission lines, which are always narrow, as they are produced in low-density regions), while the Seyfert II present only narrow emission lines. Finally, elliptical galaxies also host super-massive black holes, with a significant radio emission, but their spectra is very distinct from star-forming galaxies (Figure 14 – $left$ panel).

Thus, while broad-emission line and typical elliptical-galaxies AGN are easy to distinguish from star-forming galaxies, that is not the case for seyfert II AGN. Nevertheless, while these galaxies present only narrow emission lines in their spectra, the ionizing source (AGN) is significantly different from OB stars (in star-forming galaxies), and this has a clear effect in the flux ratios of forbidden and Hydrogen lines. Particularly, [NII], [SII], [OII] and [OIII] emission lines are usually used, together with Hβ and/or Hα to distinguish between seyfert II and star-forming galaxies. An example can be found in Figure 14 ($right$ panel).

Tab. 2: A summary of the most used star-formation rates, highlighting its strenghts and weaknesses

SF indicator	Sensitivity ($M_\odot yr^{-1}$)	Extinction (mag)	Delay (Myr)	Techniques	Coverage (*typical*)
GRB	100	–	300	Detection	$4 < z < 7$
X-rays	30	–	200	Imaging	$z < 0.5$
UV	0.1	1-3	10-50	Imaging	$1 < z < 7$
u-band	0.5	1-3	30-200	Imaging	$0 < z < 4$
[OII]	10	1-2	20	Spec/NB	$z < 4.5$
Hβ	20	1-2	20	Spec/NB	$z < 3$
Hα	1	0.5-1	20	Spec/NB	$z < 2.5$
Pa-α	10	0.5	20	Spec/NB	$z < 0.5$
FIR	30	0	40	Imaging	$z < 2$
Sub-mm	50	0	40	Imaging	$1 < z < 6$
Radio	20	0	200	Imaging	$z < 1.5$

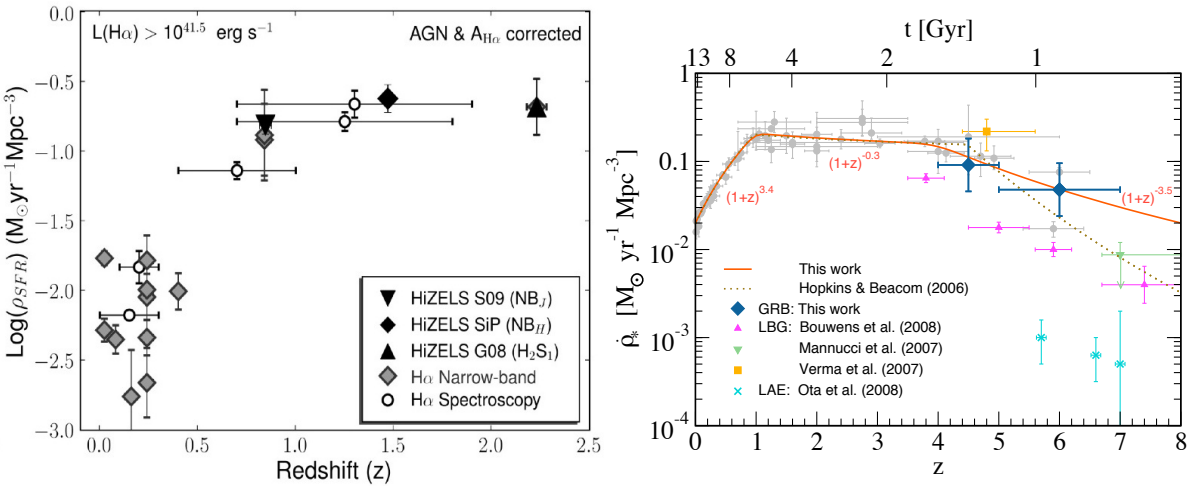

Fig. 15: Evolution of star formation rate density as traced by present surveys of Hα emitters (Sobral et al. 2009) (*left*). This shows the star formation density estimated from reddening-corrected Hα observations. The *right* panel presents the evolution of the star formation rate density as traced by present surveys using several SF tracers, including the latest estimates from gamma-ray bursts (from Yuksel et al. (2008).

3 Aplication: The Star Formation History of the Universe

3.1 The Star Formation History *today*

Using all the star-formation tracers described in the previous sections it is possible to construct an estimation of the actual star-formation history of the Universe, from the local Universe up to the highest redshifts that we are able to probe in the present. These surveys show that the star-formation rate density rises as $(1+z)^4$ – or possibly higher – out to at least z∼1 (e.g. Sobral et al., 2009) indicating that most of the stars in galaxies today formed at z $>$ 1 with the peak occurring around that cosmic time. However, determining the precise redshift where the star-formation rate peaked is not trivial, especially when different star-formation indicators give different measures of the integrated star-formation rate density. Nevertheless, the star-formation rate density seems to flatten at z $\sim$ 2 and thus it is likely that the majority of stars seen today were indeed formed between z $\sim$ 1 and z $\sim$ 3. Also, z∼ 2-2.5 appears to be an important era in the evolution of many populations, such as Quasi Stellar Objects (QSOs) and sub-millimeter galaxies, which may be intimately linked to the formation of massive galaxies. However, it is still not completely certain if the evolution of $\rho*$ reaches a peak around z∼1.5 and decreases significantly thereafter or whether it stays flat to much higher redshifts.

4 Appendix

Cosmology and Cosmography

No matter where we look at in the Universe, we cannot escape its immense structure and diversity. From our solar system to clusters and super clusters of galaxies, the universe reveals a complex pattern on almost every scale we have observed. In fact, it is only when we observe the large scale structure, or look way back in time that we see that the Universe is in fact quite close to being homogenous and isotropic. On the other hand, by studying the universe as it was thousands of millions of years ago, we also understand that its structure is immensely dynamic and always evolving. Thus, the triumph of Cosmology over the past century has been to model with accuracy what we see and observe in our Universe, particularly with the Λ Cold Dark Matter model.

General Relativity

Einstein's field equations describe how energy, being equivalent to mass, affects space and time, making use of the covariance principle (according to the Lorentz transformations). The field equations are:

$$R_{\mu\nu} - \frac{R}{2} g_{\mu\nu} + \Lambda g_{\mu\nu} = -\frac{8\pi G}{c^4} T^{\mu\nu} \tag{6}$$

where $R_{\mu\nu}$ is the Ricci tensor (the contraction of the curvature tensor), R its contraction (the curvature scalar), $g_{\mu\nu}$ is the metric tensor and $T^{\mu\nu}$ is the energy-momentum tensor. Finally, Λ is the cosmological constant, G is Newton's gravitational constant and c is the speed of light.

Assuming that the universe is homogeneous and isotropic, one gets a simplification of the metric of the universe. It may be described by the line element ds of the Robertson-Walker metric in polar coordinates x^{μ}=(t, r, θ, ψ) as:

$$ds^2 = dt^2 - a(t)^2 \left[\frac{dr^2}{1 - kr^2} + r^2 (d\theta^2 + \sin^2 \theta d\phi^2) \right] \tag{7}$$

where $a(t)$ is the scale factor (time dependent) which describes an expanding universe. On the other hand, k, the curvature of space, may be set to k = 0, +1 or -1 by choosing an appropriate scaling of r.

One may describe matter in the universe as a continuous ideal fluid consisting of particles (such as galaxies) which have a mean matter density $\rho(t)$ and a pressure $P(t)$. Evaluating for today ($t = t_0$), one can introduce the following constants:

$$a_0 = a(t_0), \qquad H_0 = \frac{\dot{a}(t_0)}{a(t_0)}, \qquad \rho_0 = \rho(t_0), \qquad q_0 = -\frac{\ddot{a}(t_0) a(t_0)}{\dot{a}(t_0)^2} \tag{8}$$

where q_0 is the deceleration parameter and H_0 is the Hubble constant. Today the universe is matter-dominated, which means $\rho_{rad} \sim 0$. Using all this, one may evaluate the curvature of space expressed in the above constants:

$$\frac{k}{a_0^2} = H_0 \left(\frac{3}{2} \frac{\rho_0}{\rho_{cr}} - q_0 - 1 \right) \tag{9}$$

where

$$\rho_{cr} = \frac{3H_0^2}{8\pi G} \tag{10}$$

is the critical density. Finally, it is important to introduce the density parameters:

$$\Omega_M = \frac{\rho_0}{\rho_{cr}} = \frac{8\pi G \rho_0}{3H_0^2}, \qquad \Omega_\Lambda = \frac{\Lambda}{3H_0^2}, \qquad \Omega_k = 1 - \Omega_M - \Omega_\Lambda \tag{11}$$

The cosmological parameters H_0, Ω_m, Ω_Λ and k are subject to numerous measurements. The latest values have been derived from type Ia supernovae brightness measurements (Perlmutter et al., 1999) and from the power spectrum of the cosmic microwave background (CMB) with WMAP (Spergel et al., 2003). Throughout this document, a "F737" cosmology will be used, meaning:

$$k = 0, \qquad H_0 = 70 \text{ km.s}^{-1}\text{Mpc}^{-1}, \qquad \Omega_M = 0.3, \qquad \Omega_\Lambda = 0.7 \tag{12}$$

On the other hand, it is clear today that the baryonic matter we can see directly (as stars or illuminated by stars) or indirectly (absorption) accounts for at most $\frac{1}{10}$ of Ω_M (Springel et al., 2005). The dynamic properties of galaxies and galaxy clusters and the effects of gravitational lensing agree well with such result, while the discovery of the Bullet cluster (1E 0657-56) (Markevitch et al., 2002) and subsequent study (Markevitch et al., 2004) clearly points towards the existence of $dark\ matter$, which, to date, we have not been able to clearly identify.

The Hubble constant H_0 has been mentioned before, but it has not been clearly defined. It is a constant of proportionality between recession speed v and distance d in the expanding Universe:

$$v = H_0 d \tag{13}$$

The subscripted 0 refers to the present epoch, as in general H changes with time. H_0 has inverse time dimensions, but it is usually written as:

$$H_0 = 100h \text{ km.s}^{-1}\text{Mpc}^{-1} \tag{14}$$

where h is a dimensionless number. As referred before, we assume h=0.7, which is in good agreement with recent observations. The inverse of the Hubble constant is the Hubble time $t_H = \frac{1}{H_0}$ and the speed of light c times the Hubble time is defined as the Hubble distance $D_H = \frac{c}{H_0}$. These are the quantities that set the scale of the Universe.

With an expanding Universe, computing distances turns out to be slightly more complex than in a simple euclidean non-expanding universe. In fact, this expansion (and possible curvature) makes distances between comoving objects change constantly.

Redshift

One of the most common ways to describe large astronomical distances is by the concept of redshift. Observations show that for distances larger than $\sim$ Mpc the more distant an object is, the more its light is shifted to longer wavelengths. Absorption and emission lines of atoms are commonly used to measure a redshift. The redshift effect may be explained in two ways. One may interpret it as the Doppler effect that affects light due to the movement of the source relative to the observer. The other way to look at it is a general expansion of space which stretches the light wave (cosmological redshift). The redshift, z, is defined as:

$$z = \frac{\lambda_0 - \lambda_\epsilon}{\lambda_\epsilon} \tag{15}$$

where λ_0 is the observed wavelength and λ_ϵ is the wavelength of the photon in the rest-frame of the source. The redshift is related to the scale factor $a(t)$ of the universe:

$$1 + z = \frac{a(t_0)}{a(t_\epsilon)} \tag{16}$$

where $a(t_0)$ is the size of the Universe at the time the light from the object is observed, and $a(t_\epsilon)$ is the size at the time it was emitted. Redshift is independent of cosmology, but it definitely does not correspond to a distance one could measure with a ruler. To obtain a distance measure in a proper length scale, one needs to take spacetime into account, for which there are many ways, as defined in the next sections.

Line-of-Sight Co-moving Distance

As light needs time to get from an object to the observer, one can define a distance that may be measured between the observer and the object with a ruler at the time the light was emitted, the proper distance. The proper distance evaluated for today is called the $co\text{-}moving\ distance$. To obtain this quantity, one can consider a beam of light emitted along the line of sight between the object and the observer. It is emitted at the time t_e from the object and is received by the observer today, i.e., at $t = t_0$. The light thus runs a distance cdt, which is stretched as the universe expands. Integrating all those small distances leads to the line-of-sight co-moving distance:

$$D_C = \int_{t_e}^{t_0} c\frac{a_0}{a(t)}\mathrm{d}x \tag{17}$$

The co-moving distance between two nearby objects in the Universe is the distance between them which remains constant with epoch if the two objects are moving with the Hubble flow. The total line-of-sight co-moving distance D_C from us to a distant object is computed by integrating the infinitesimal δD_C contributions between nearby events along the radial ray from z = 0 to the object. On the other hand, by defining the function:

$$E(z) = \sqrt{\Omega_M(1+z)^3 + \Omega_k(1+z)^2 + \Omega_\Lambda} \tag{18}$$

the total line-of-sight co-moving distance is then given by integrating those contributions:

$$D_C = D_H \int_0^z c\frac{dz'}{E(z')} \tag{19}$$

where D_H is the Hubble distance.

As most of the distance measurements can be derived from the line-of-sight co-moving distance, it can be considered as a fundamental way of measuring distances in cosmology. Nevertheless, the previous integral does not have, in general, an analytical solution, thus a numerical solution is normally needed to solve it.

Transverse Co-moving Distance

The co-moving distance between two events at the same redshift (distance between two objects separated on the sky by some angle $d\theta$) is $D_M d\theta$ and the transverse co-moving distance D_M is equal to the co-moving (D_C) distance if we assume a flat universe.

Angular Diameter Distance

The angular diameter distance, D_A is defined as the ratio of an object's physical transverse size to its angular size (in radians). It is used to convert angular separations in telescope images into proper separations at the source. It is famous for not increasing indefinitely as z $\rightarrow \infty$. In fact, it turns over at z$\sim$ 1 and thereafter more distant objects actually appear larger in angular size. Angular diameter distance is related to the transverse co-moving distance by:

$$D_A = \frac{D_M}{1+z} \tag{20}$$

Luminosity Distance

The luminosity distance, D_L is defined by the relationship between the bolometric flux S and the bolometric luminosity L:

$$D_L = \sqrt{\frac{L}{4\pi S}} \tag{21}$$

This is related to the transverse co-moving distance and angular diameter distance by:

$$D_L = (1+z)D_M = (1+z)^2 D_A \tag{22}$$

Co-moving Volume

The co-moving volume V_C is the volume measure in which the number densities of non-evolving objects locked into Hubble flow are constant with redshift. The co-moving volume element in a solid angle $d\Omega$ and for a redshift interval dz is:

$$dV_C = D_H \frac{(1+z)^2 D_A^2}{E(z)} d\Omega dz \tag{23}$$

where D_A is the angular diameter distance at redshift z. Once again, assuming a flat universe simplifies the calculations and thus the total co-moving volume, all-sky, out to redshift z is given by:

$$V_C = \frac{4\pi}{3} D_M^3 \tag{24}$$

In general, one can write:

$$V_C = \int_{\theta_0}^{\theta_f} \int_{\phi_0}^{\phi_f} \int_{z_0}^{z_f} \frac{D_H (1+z) D_C^2}{E(z)} d\Omega dz \tag{25}$$

Look-back Time

The lookback time t_L to an object is the difference between the age t_0 of the Universe now (at observation) and the age t_e of the Universe at the time the photons were emitted (according to the object). It is used to predict properties of high-redshift objects with evolutionary models, such as passive stellar evolution for galaxies and is given by:

$$t_L = t_H \int_0^z \frac{dz'}{(1+z')E(z')} \tag{26}$$

Luminosity function

In order to calculate a luminosity function (of Hα emitters, for example), line fluxes can be converted to luminosities by applying:

$$L_{\mathrm{H}_\alpha} = 4\pi \mathrm{D}_\mathrm{L}^2 \mathrm{F} \tag{27}$$

where $\mathrm{D_L}$ is the luminosity distance, as defined before, and F is the measured flux.

The estimate of the source density in a luminosity bin of width $\Delta(\log L)$ centered on $\log L_c$ is given by the sum of the inverse volumes of all the sources in that bin. Therefore, the value of the source density in that bin is

$$\phi(\log(L_c)) = \frac{1}{\Delta(\log L)} \sum_{|\log \frac{L_i}{L_c}| < \frac{\Delta(\log L)}{2}} \frac{1}{\Delta(V_{\mathrm{filter}})}. \tag{28}$$

Here, i refers to sources and c to the center of each bin. The volume probed is calculated taking into account the nature of the survey.

The luminosity functions are then usually fitted with a Schechter function defined by the three parameters: α, ϕ^* and L^*:

$$\phi(L)dL = \phi^*(L/L^*)^\alpha \exp(-L/L^*) d(L/L^*). \tag{29}$$

The integral of the luminosity function can then be directly transformed into an average star-formation rate density at a specific epoch.

References

Buat V., Xu C., 1996, A&A, 306, 61

Ibar et al. 2008, MNRAS, 386, 953

Kennicutt Jr. R. C., 1998, ApJ, 498, 541

Kennicutt Jr. R. C., Tamblyn P., Congdon C. E., 1994, ApJ, 435, 22

Madau P., Pozzetti L., Dickinson M., 1998, ApJ, 498, 106

Markevitch M., Gonzalez A. H., Clowe D., Vikhlinin A., Forman W., Jones C., Murray S., Tucker W., 2004, ApJ, 606, 819

Markevitch M., Gonzalez A. H., David L., Vikhlinin A., Murray S., Forman W., Jones C., Tucker W., 2002, ApJL, 567, L27

Miller G. E., Scalo J. M., 1979, ApJ, 41, 513

Perlmutter et al. 1999, ApJ, 517, 565

Salpeter E. E., 1955, ApJ, 121, 161

Scalo J. M., 1986, Fundamentals of Cosmic Physics, 11, 1

Sobral et al. 2009, astro-ph/0901.4114, MNRAS $in\ press$

Spergel et al. 2003, ApJs, 148, 175

Springel et al. 2005, Nature, 435, 629

Yuksel H., Kistler M. D., Beacom J. F., Hopkins A. M., 2008, astro-ph, 804

.